Interaction of oxygen and carbon monoxide with Pt(111) at intermediate pressure and temperature : revisiting the fruit fly of surface science

Bashlakov, D.

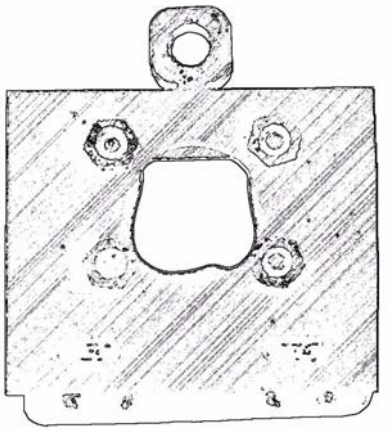

Chapter 2

Experimental instruments and techniques

In surface science, experiments are conducted in a well-controlled environment. Ultra high vacuum (UHV) conditions are often used for sample preparation and characterization. Results presented in this thesis were collected using two UHV instruments: The "Omicron" system (Chapters 3, 4 and 5) and the "Lionfish" system (Chapter 3). Both systems contain equipment for cleaning of single crystal surfaces and for characterization with surface sensitive techniques. These techniques are described in this chapter. High purity $^{16}O_2$ (Messer 5.0), Ar (Messer 5.0), CO (Air Liquide 4.7), and $^{18}O_2$ (Cambridge Isotope Laboratories, 97% isotope purity and ≥99.9 chemical purity) were used for sample cleaning and gas dosing.

2.1 The Omicron system

The Omicron system's principal surface sensitive technique is Scanning Tunneling Microscopy (STM). Auger Electron Spectroscopy (AES) and LEED are supporting techniques used for surface characterization. The system consists of two UHV chambers, one load lock and a set of manipulators for sample/tip transfer. A custom made gas mixing manifold is connected by separate dosing lines to each of the UHV chambers. The pressure in the gas lines can be reduced to below 10^{-3} mbar prior to filling them with gases.

2.1.1 Vacuum system

The preparation and analysis chambers both have a base pressure of $\approx 2 \times 10^{-10}$ mbar as monitored with Bayard-Alpert type manometers. A gate valve separates the chambers. Both chambers can be evacuated using a combination of an ionization pump (Varian, Star Cell) and a turbo molecular pump (Pfeiffer, TMU-260). Gate valves allow for pumping on each chamber by either pump. The turbo molecular pump is switched off prior to STM measurements to reduce vibrations in the system. Similarly,

ionization pumps were switched off during sample cleaning and experiments involving oxygen doses.

The preparation chamber is equipped with leak valves and an ion gun for sample cleaning. This includes sputtering with argon ions and subsequent annealing of the sample. Single crystals are mounted in a sample holder with a built-in tungsten filament that faces the back side of the sample. The filament has electrical contacts which are isolated from the rest of the sample holder. It allows for radiative heating and electron bombardment heating from room temperature up to 1200 K. To this purpose, the preparation chamber has a manipulator with electrical connections to the sample holder's filament and thermocouple.

The analysis chamber is equipped with an Omicron variable temperature (VT) STM, a rear view LEED apparatus (VG RVL-900), an electron gun (VG LEG 63), a hemispherical electron analyzer for Auger spectroscopy (VG 100 AX), and a storage unit for six sample/tip holders. Two leak valves connected to the O_2 and CO gas lines allow for separate dosing of these gases in the analysis chamber. In addition, an initially prepared O_2:CO gas mixture with required composition can be dosed by expansion from the small volume separated from the analysis chamber using a valve. An x,y,z-manipulator with 360º rotation is used for proper positioning of the sample for LEED and AES measurements.

2.1.2 Auger electron spectroscopy

AES is a surface sensitive technique used to characterize chemical composition of a sample's (near) surface. The mechanism of Auger electron emission is as follow. When surface atoms are bombarded by high energy electrons or photons, they can eject an electron from a core level of an atom and create a hole. This hole is filled by an electron from a higher energy level. The released energy may be transferred to a third electron, If this one is ejected into vacuum, it is called an Auger electron. The energy of Auger electrons depends only on the nature of the atom that emits them. Therefore, elemental analysis can be performed by measuring the energy spectrum of Auger electrons and comparing it to handbook spectra [1, 2].

In our system, a beam of electrons with 3 keV kinetic energy is used to produce Auger electrons. Energy spectra are recorded with a hemispherical electron energy analyzer. Carbon was found as the main contamination for samples introduced into the system. Sensitivity of the Auger spectrometer was tested for carbon and oxygen on the clean Pt(111) surface covered with

0.5 ML of CO. The lower sensitivity range was not determined due to the poor control over the dosing for smaller coverage. That is why a final evaluation of the surface quality was done with STM.

2.1.3 Low energy electron diffraction

In contrast to Auger spectroscopy, LEED technique is based on the elastic scattering of electrons. These electrons have a de Broglie wavelength λ defined by

$$\lambda = \frac{h}{\sqrt{2mE}}, \quad (2.1)$$

where h is Plank's constant, m is the mass of an electron and E is the electron energy. To calculate the wavelength in nanometers, equation (2.1) is also used in the form

$$\lambda(nm) = \sqrt{\frac{1.5}{E(eV)}}. \quad (2.2)$$

Therefore, for electrons with energies between 50 and 200 eV, which is typical in diffraction experiments, λ=0.2-0.1 nm. This is comparable to interatomic distances. In LEED, the primary beam of electrons with fixed energy impinges onto a single crystal surface. Back-scattered electrons pass through electrostatic grids that select only the elastically scattered electrons. These are visualized on a hemispherical phosphorous screen. Constructive interference between the electrons results in a diffraction pattern on the screen. The pattern represents an image of the reciprocal lattice of the real surface. In reciprocal space, diffraction from a periodic structure follows the Laue condition, which is expressed in the following form for a two dimensional lattice [3]:

$$\vec{k}_{||} - \vec{k}'_{||} = m\vec{a}^* + l\vec{b}^*, \quad (2.3)$$

Here, $\vec{a}^*$ and $\vec{b}^*$ are the basis vectors of the surface in reciprocal space, m and l are integers, $\vec{k}_{||}$ and $\vec{k}'_{||}$ are the components of a wave vector parallel to the surface for incident and scattered electrons, respectively. In the case of elastic scattering:

$$\left|\vec{k}\right| = \left|\vec{k}'\right| = \frac{2\pi}{\lambda}, \quad (2.4)$$

The basis vectors of the reciprocal lattice expressed via the real space basis vectors $\vec{a}$, $\vec{b}$ and the unit vector normal to the surface $\vec{n}$:

$$\vec{a}^* = \frac{2\pi \vec{b}\vec{n}}{\vec{a}(\vec{b}\times\vec{n})} \quad \text{and} \quad \vec{b}^* = \frac{2\pi \vec{n}\vec{a}}{\vec{a}(\vec{b}\times\vec{n})}, \text{(2.5)}$$

or:

$$a^* = |\vec{a}^*| = \frac{2\pi}{a\sin(\angle \vec{a}\vec{b})} \quad \text{and} \quad b^* = |\vec{b}^*| = \frac{2\pi}{b\sin(\angle \vec{a}\vec{b})}. \text{(2.6)}$$

The $\sin(\angle \vec{a}\vec{b}) = S$ reflects the symmetry of the surface lattice, which can be rectangular (S=1) or hexagonal (S=√3/2). In case of an incident electron beam normal to the surface for the (10) diffraction spot (m=1, l=0) the combination of equations (2.3), (2.4) and (2.6) gives:

$$\frac{2\pi}{\lambda}\sin(\theta) = \frac{2\pi}{aS}, \quad \text{or} \quad aS\sin(\theta) = \lambda \text{ (2.7)}$$

Therefore, the unit cell of an unknown surface lattice can be calculated from the LEED image, since the electron wave length (λ) is given by equation 2.2, S can be assumed from the symmetry of the LEED image, and sin(θ) for the diffraction spots is defined from the dimensions of LEED optics. In case the sample is placed in the geometrical center of the hemispherical LEED screen (Figure 2.1a):

$$\sin(\theta) = \frac{C}{R}; \text{(2.8)}$$

where R is the radius of curvature of the LEED screen and C is the distance from the center of LEED image to the diffraction spot. This equation cannot be applied if the sample is displaced from the geometrical center of the LEED optics as illustrated in Figure 2.1c. In Chapter 4 the period for the CO adlayer on the Pt(111) surface is calculated. The platinum diffraction pattern is used to calculate the displacement of the sample D=L-X (Figure 2.1b). By using the distance between platinum atoms (a=2.77 Å), equation (2.7),

$$\varphi = \arcsin\left(\frac{2\lambda}{\sqrt{3}a}\right), \text{(2.9)}$$

and trigonometric equations

$$tg(\varphi) = \frac{A}{L} \text{ (2.10)}$$

and

$$X = \sqrt{R^2 - A^2}\ , \quad (2.11)$$

the displacement D can be calculated from:

$$D = \frac{A}{tg(\arcsin(\frac{2\lambda}{\sqrt{3}a}))} - \sqrt{R^2 - A^2} \quad (2.12)$$

The angle θ for the diffraction maximum of an unknown structure *C'* (Figure 2.1c) can be calculated from

$$\theta = arctg(\frac{C'}{D + \sqrt{R^2 - C'^2}})\ . \quad (2.13)$$

In Chapter 4, the described expression (2.13) of a reflection angle θ placed into equation (2.7) is used to determine the period of a Moiré pattern for the CO adlayer.

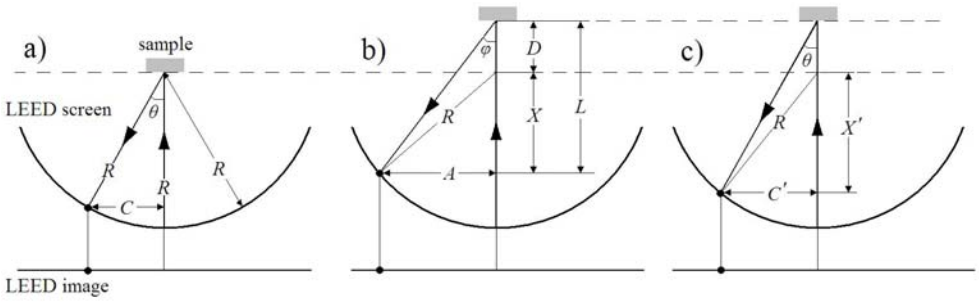

Figure 2.1 Schematic representation of a LEED experiment for a sample placed in the center of the LEED optics (a), or displaced by the distance D from it (b, c). The large arrows mark the incoming and the back-scattered beams of electrons.

2.1.4 Scanning tunneling microscopy

The interpretation of LEED images is not always straightforward. Adsorbed molecules can arrange in domains with different orientations relative to the substrate and each of these will contribute to the LEED pattern. The power of scanning tunneling microscopy (STM) is that the

surface structure can be visualized locally with atomic resolution, thus any ambiguity about the adsorbate's arrangement can be ruled out [4]. The STM technique employs the effect of tunneling of electrons through the potential barrier created between an atomically sharp metal tip and a conductive surface. The tunneling current I_t can be detected when the tip approaches the surface and some voltage V_t is applied between them. The conductivity G of the tunnel barrier is [5]:

$$G = \frac{I_t}{V_t} \approx \exp(-2\kappa z) \cdot \rho(r_t, E_F) \text{ , (2.14)}$$

where z is the tip-to-sample distance, κ is the decay constant for the electron wave function in vacuum and ρ is the local density of states of the surface at the Fermi level (E_F) in the position of the tip r_t. Spatial changes in the local electron density of states follow the arrangement of the surface atoms. By moving the tip across the surface in x,y direction while adjusting the tip position to keep the tunnel current constant (constant current mode) and recording the z position of the tip, the topography of the surface can be measured with atomic resolution.

The sensitivity of the STM technique is governed by decay constant κ:

$$\kappa = \frac{\sqrt{2m\Phi}}{h} \approx 11 nm^{-1} \text{ , (2.15)}$$

were h is Planck's constant, m is the mass of an electron and Φ is the height of the potential barrier, which is equivalent to the work function of materials used in the STM experiment [6]. Using this value for the decay constant in equation (2.14), the tunnel current ratio at the same x,y tip position for different tip-to-surface distances is

$$\frac{I_t^I}{I_t^{II}} = \exp(-22(z^I - z^{II})) \text{ , (2.16)}$$

The corrugation of the local density of states on metal surfaces is in the range of 5 to 20 pm [6]. Thus, changes in tunnel current of 10-50% should be detectable to measure the surface topography with atomic resolution. In other words, the contribution into the tunnel current from parasitic signals should be less then 10% for "flat" surfaces not to override the current variations caused by the surface topography. The origins of parasitic signals are typically mechanical vibrations and electronic crosstalk. To improve the resolution of any STM system, both components should be reduced to a minimum. Passive damping of external vibrations in the Omicron system

was realized by mounting the UHV set-up on a special floor that is decoupled from the rest of the building. Additional damping of vibrations was realized with an Eddy current damping stage on the STM scanner. It is hanging on springs inside the UHV chamber. Electronic crosstalk from external sources was effectively screened by the UHV chamber serving as a Faraday cage. In addition, grounding of electronic equipment to a common ground point prevents parasitic crosstalk into the tunnel current measurement circuit from the rest of the system.
Beside external factors that influence resolution, a highly important factor is the interaction of the tip with the surface. It has been observed experimentally that the ability to resolve every single atom on the surface depends on the tip state and geometry [6]. Preparation of an atomically sharp tip is an intricate part of the STM experiment itself. The results presented in Chapters 3, 4 and 5 were obtained with self-prepared tungsten tips. These tips were electrochemically etched in the loop-meniscus configuration (Figure 2.2a) from a 0.25 mm tungsten wire in a 2M solution of NaOH and with a platinum counter electrode. The bottom part of the wire was caught and used as a tip. The shape of the prepared tips was characterized in a scanning electron microscope (FEI Nova SEM). An etching routine of applying a DC voltage $\geq$3V gave the most reproducible results: a single tip apex of 10-50 nm radius and a smooth finish of the tungsten surface (Figure 2.2b). At the same time, etching with a DC voltage <2V or with an AC voltage often led to the formation of a rough tungsten surface, probably due to the uneven etching speed along different crystal planes. As a result, multiple apex tips were regularly produced, as shown in Figure 2.2c. The sharpest tips were selected and mounted into the tip holder shown in the inset of Figure 2.2d.

The tungsten oxide formed during etching has to be removed prior to using tips for scanning [7]. The tip apex was heated in an UHV environment by an emission current up to 200 μA. This treatment yields a stable electron emission current in the 0-20 nA range, as shown in Figure 2.2d and a stable tunnel current under tunneling conditions.

Subsequent conditioning of the tips included scanning of an Au(100) single crystal surface. The advantage of using a gold sample is twofold:

- the gold surface stays almost indefinitely clean under UHV conditions;
- it is much easier to resolve the structure of the quasi-hexagonal reconstruction of the Au(100) surface (z corrugation ≈0.5Å) than the atomic fine structure (corrugation ≈0.1 Å) [8].

All tips that showed stable emission current were able to resolve the reconstruction on the gold surface. To improve the spatial resolution further, pulses of a voltage of 2-3 V were applied over the tunnel junction. This treatment leads to restructuring of atoms on the tip apex and to improvement of the tip resolution. Tip conditioning was performed daily until the fine structure of the Au(100) surface was observed (Figure 2.3c).

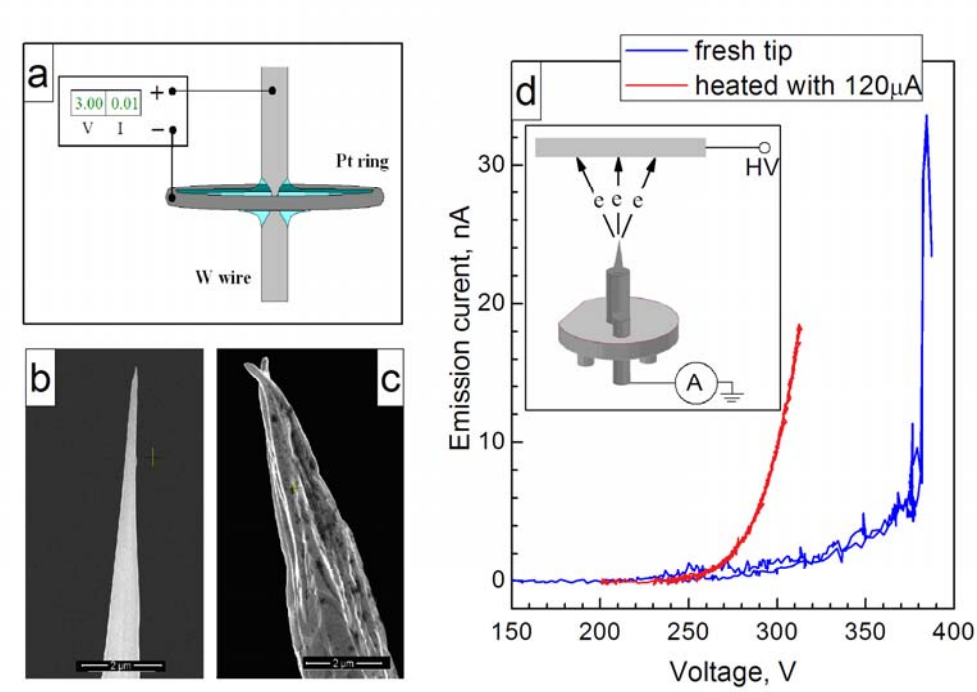

Figure 2.2 Stages of STM tip preparation for the Omicron system. Electrochemical etching in 2M NaOH solution (a). Validation of the tip geometry with SEM (b, c). (d) Tip conditioning inside the UHV chamber by an emission current induced through applying a high voltage between the tip and a counter electrode as shown in the inset. The I(V) emission curve in the 0-20 nA range for a fresh tip (blue line), and for the same tip after being heated with 120 μA of emission current (red line).

2.1.5 Sample preparation

Au(100)

A 1 mm thick flat gold single crystal with a 5x7 mm^2 elliptical shape exposing a polished (100) plane [9] was cleaned in the UHV system by several cycles of

- argon sputtering for 10 min at 600eV ion energy and 5-8 μA ion current;
- annealing in vacuum at 700-720 K for 5 min.

This procedure removes the initial contamination (carbon and sulfur, Figure 2.3a) and gives an STM-grade clean surface as shown in Figures 2.3 b and c.

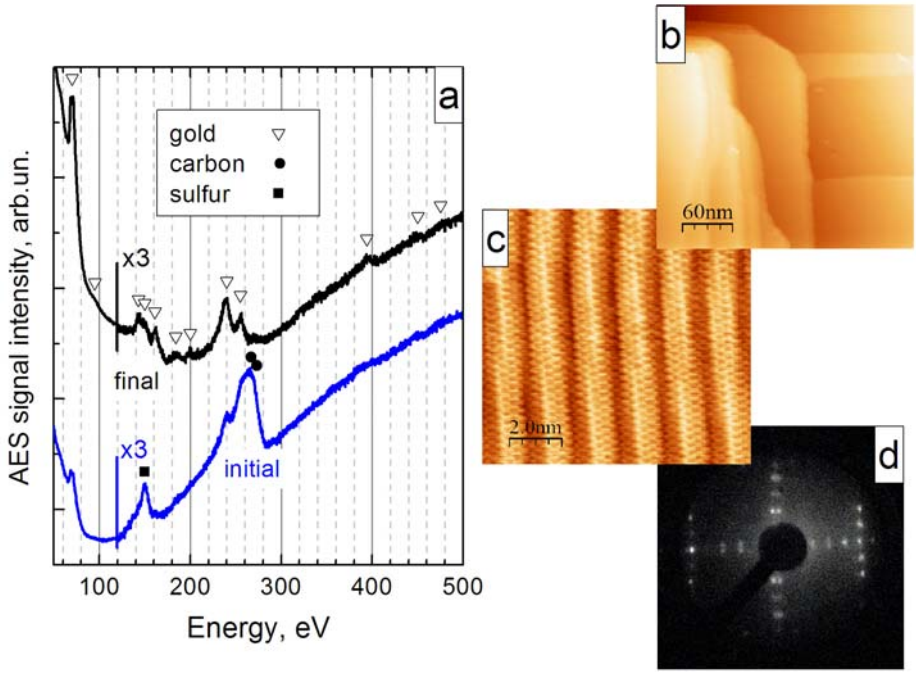

Figure 2.3 Validation of the quality of the Au(100) surface. Auger spectrum of the surface composition before (blue line) and after (black line) sputtering-annealing cycles (a). STM image of the 260x260nm^2 surface area (b) and 8.6x8.6nm (c) for a clean surface. Fine structure of the quasi-hexagonal reconstruction observed with LEED at 60eV primary electron beam energy (d).

Pt(111)

STM data presented in Chapters 3-5 were collected using a 1 mm thick 6 mm diameter circular single crystal mechanically polished along a (111) plane [9]. The sample was cleaned with several cycles of

- argon sputtering for 10 min at 800-1000 eV ion energy and 8-12 μA ion current;
- heating for 10-30 min in 3-6x10^{-7} mbar of oxygen at 800-900 K to remove carbon, or annealing to 1100-1200 K in vacuum for 5 min.

The quality of the cleaning procedure was first verified by Auger spectroscopy (Figure 2.4a). After contamination levels dropped below the detection level of AES, the quality of the surface was monitored with STM. Sputtering-annealing cycles were repeated until an atomically-resolved, STM-clean surface was observed (Figure 2.4c). The daily cleaning routine included annealing in oxygen for half an hour and flashing to 1200 K in vacuum.

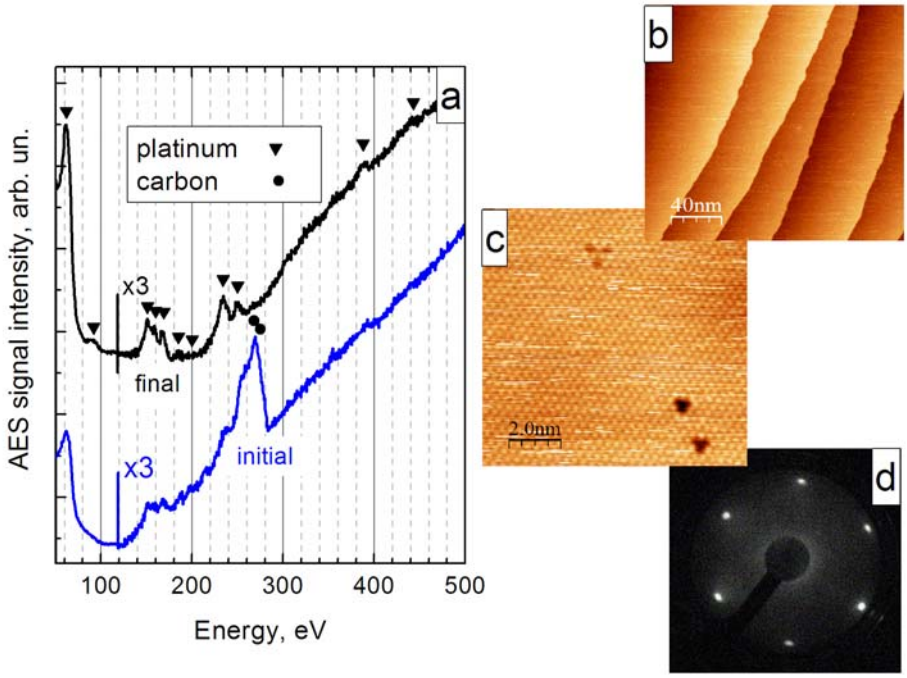

Figure 2.4 Validation of the quality of the Pt(111) surface. Auger spectrum for the surface composition before (blue line) and after (black line) the sputtering-annealing cycles (a). STM topography of the 170x170nm surface area (b) and 8.6x8.6nm (c) for a clean surface. LEED image of the STM grade clean Pt(111) surface taken at the 68 eV beam energy (d).

2.2. Lionfish

2.2.1 Vacuum system

The results of the TPD and temperature programmed reaction spectroscopy (TPRS) measurements, described in Chapter 3, were obtained using a home-build instrument named "Lionfish". The system has a base pressure $<2\text{x}10^{-10}$ mbar which is achieved using two turbo molecular pumps placed in series (Pfeiffer TMU 521 and TMH 071) and a rotary vane pump (Pfeiffer Duo 10). The system hosted a 10 mm diameter and 1 mm thick platinum single crystal with one side polished to <0.1º precision of (111) plane [9]. The sample was mounted on the differentially pumped manipulator with cooling by liquid nitrogen. The sample temperature was measured by a K-type thermocouple spot-welded to the side of the crystal. The filament was placed on the back side of the crystal. Radiative heating and electron bombardment were used for the sample heating with a PID controller (Eurotherm 2416). In combination with LN_2, cooling this yielded accurate control of sample temperature between 85 and 1300 K. The system is equipped with a quadrupole mass spectrometer (Balzers Prisma 200), a rear view LEED (LK Technologies RVL2000/8/R), a sputtering gun and leak valves for background dosing.

2.2.2 Temperature programmed techniques

TPD and TPRS belong to a class of techniques in which a reaction is monitored while the temperature of a sample changes [10]. These techniques allow to evaluate the surface coverage and activation energy for desorption/recombination of surface-bound species. During an experiment, the surface is first covered with adsorbates. Then the temperature of the sample is linearly increased while the reaction products are monitored with a mass spectrometer. The concept of temperature programmed measurements is related to the Arrhenius equation for the reaction rate, r

$$r = A\exp(\frac{E}{kT}) \text{ , (2.17)}$$

The desorption processes is described by the Polanyi-Wigner equation [11]:

$$r(t) = -\frac{d\theta}{dt} = \nu\theta^n(t)\exp(\frac{E}{RT}) \text{ , where } T = T_0 + \beta t \text{ , (2.18)}$$

where r is the rate of desorption, t is time, ν is the pre-exponential factor, θ is the adsorbate coverage, n is order of desorption process, t is the time, E is activation energy of desorption, R is the gas constant, and T is the sample temperature which increases with the heating rate β. The number of molecules leaving the surface is detected as a change of the partial pressure

P relative to the steady state background partial pressure in the vacuum system for the molecule of interest

$\Delta P(t) \sim r(t)$.

As can be seen from (2.18), the pressure will increase first since the probability for the molecules to leave the surface increases while the temperature rises. At some point, the decrease in the surface coverage ceases to allow further pressure rise. ΔP goes through a maximum and drops to zero when all adsorbed species have left the surface. The position of the maximum and the shape of the TPD spectra contain information about the activation energy and the order of the desorption process [12]. The area under the TPD spectrum is proportional to the surface coverage:

$$\theta = \int_0^{t\_\max} \frac{d\theta}{dt} dt \sim \int_0^{t\_\max} \Delta P(t) dt = \int_{To}^{T\max} \Delta P dT \quad . \quad (2.19)$$

Hence, with the proper system calibration, the surface coverage of the adsorbed species can be determined from the measured spectrum. In Chapter 3, various coverages of atomic oxygen were determined from the area of TPD spectra by comparing them to the TPD peak area of the O-p(2x2)Pt(111) layer with 0.25 ML coverage.

2.2.3 Sample preparation

The (111) surface of this Pt single crystal was cleaned with repeated cycles of Ar sputtering (600eV, 0.2-0.3 μA) for 15 min, annealing in oxygen atmosphere (1-3x10^{-7} mbar) at 900-1000 K for 5 min and annealing in vacuum at 1200 K for 5 min. LEED from the clean surface revealed a hexagonal diffraction pattern similar to what had been observed for a clean Pt(111) surface in the Omicron system (Figure 2.5).

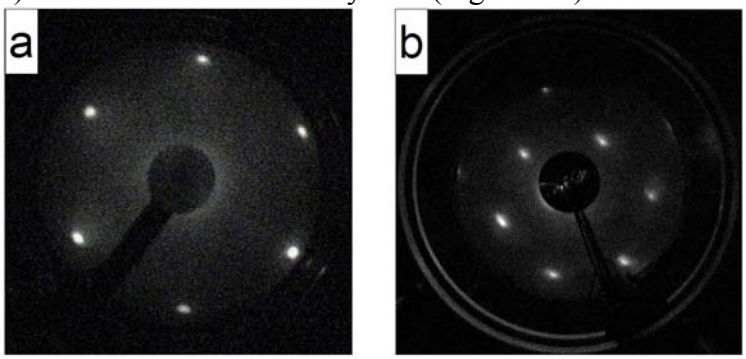

Figure 2.5 LEED images of two platinum single crystals with (111) plane from Omicron (a) and Lionfish (b) systems taken with 68 eV and 100 eV beam energy, respectively.

No additional structure was detected, although the diffraction spots show some elongation. This is ascribed to imperfect focusing of the electron beam.

The chemical quality of the surface was checked by tracing the TPD signals of CO, CO_2 and water after the surface was exposed to oxygen at 85 K. This procedure verifies for the absence of main contaminants on the platinum surface, which are residual carbon or CO and H_2 adsorbed from the residual gas in the UHV chamber. These sources of contamination will react with oxygen and form CO, CO_2 and H_2O which desorb from the surface in temperature intervals 300-500 K, 200-350 K and 150-200 K, respectively. None of such desorption peaks were detected (Figure 2.6 b). A peak in the CO signal at 100 K is due to CO desorption from the filament. The same is true for a peak observed near 100 K for oxygen in Figure 2.6a.

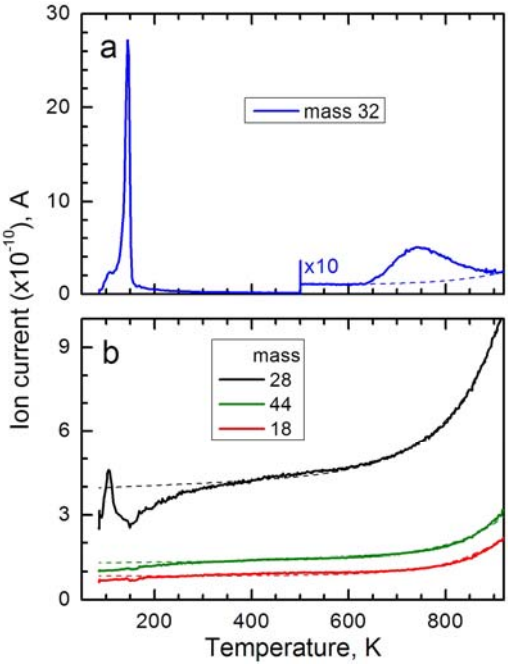

Figure 2.6 TPD traces of oxygen (a); carbon monoxide (mass 28), carbon dioxide (mass 44) and water (mass 18) (b) recorded after Pt(111) surface has been exposed to oxygen at 85 K. The dotted line shows the fit for the background signals calculated by formula (2.20)

All three masses in Figure 2.6b demonstrate a gradual increase with temperature. This is ascribed to increased heat transfer from the filament to the manipulator, which stimulates desorption of condensed residual gas and therefore increases the partial pressure of these molecules. From Figure2.6b one can see that above 300 K the increase of the background signal can be fitted with the formula:

$$Bg(T) = C\exp(T) + BT + A \text{ , (2.20)}$$

where C, B, and A are fitting parameters. This formula is used in Chapter 3 to subtract the background signal from the oxygen TPD spectra.

References:

[1] P. W. Palmberg, G. E. Riach, R. E. Weber, and N. C. MacDonald, Handbook of Auger Electron Spectroscopy, Physical Electronics Industries, Inc., Minneapolis, 1972.

[2] K. W. Kolasinski, Surface Science: Foundation of Catalysis and Nanoscience, Wiley, West Chester, 2008.

[3] F. Jona, J. J. A. Strozier, and W. S. Yang, Reports on Progress in Physics 45 (1982) 527.

[4] K. Heinz and L. Hammer, The Journal of Physical Chemistry B 108 (2004) 14579.

[5] F. Besenbacher, Reports on Progress in Physics 59 (1996) 1737.

[6] C. J. Chen, Introduction to Scanning Tunneling Microscopy, Oxford University Press, New York, 2008.

[7] S. Ernst, S. Wirth, M. Rams, V. Dolocan, and F. Steglich, Science and Technology of Advanced Materials 8 (2007) 347.

[8] C. Bombis and H. Ibach, Surface Science 564 (2004) 201.

[9] Single crystals supplied by Surface Preparation Laboratory (http://www.surface-prep-lab.com/)

[10] J. W. Niemantsverdriet, Spectroscopy in Catalysis: An introduction, Wiley-VCH Verlag GmbH, Eindhoven, 2000.

[11] D. A. King, Surface Science 47 (1975) 384.

[12] A. M. de Jong and J. W. Niemantsverdriet, Surface Science 233 (1990) 355.